

Graphene Q-switched distributed feedback fiber lasers with narrow linewidth approaching the transform limit

B. C. YAO,^{1,2} Y. J. RAO,^{1,6} S. W. HUANG,² Y. WU,¹ Z. Y. FENG,³ C. CHOI,² H. LIU,² H. F. QI,⁴ X. F. DUAN,³ G. D. PENG,^{4,5} AND C. W. WONG^{2,7}

¹Key Laboratory of Optical Fiber Sensing and Communications (Education Ministry of China), University of Electronic Science and Technology of China, Chengdu 610054, China

²Mesoscopic Optics and Quantum Electronics Laboratory, University of California, Los Angeles, CA 90095, USA

³Department of Chemistry and Biochemistry, University of California, Los Angeles, CA 90095, USA

⁴Shandong Key Laboratory of Optical Fiber Sensing Technologies, Laser Institute of Shandong Academy of Sciences, Jinan 250014, China

⁵School of Electrical Engineering and Telecommunications, University of New South Wales, NSW, 2052, Australia

⁶yjrao@uestc.edu.cn

⁷cheewei.wong@ucla.edu

Abstract: A compact all-in-line graphene-based distributed feedback Bragg-grating fiber laser (GDFB-FL) with narrow linewidth of hundreds kHz is demonstrated and investigated in this study. Performing as an optical saturable absorber, graphene oscillates the initially kHz linewidth DFB-FL, and generates high-quality passively Q-switched pulses. Pumped with a 980 nm continuous-wave laser, the Q-switched GDFB-FL observes ~ 1 μ s pulse durations, with pulse energies up to ~ 10 nJ and approaching the transform limit. The peak power is ~ 600 times higher than the original DFB-FL laser. By optimizing the cavity design and the graphene material, it is predicted that fast Q-switched pulses with more than MHz repetition rates and sub-100 ns pulse durations are achievable. Such transform-limited Q-switched GDFB-FLs with narrow linewidth of sub-MHz have long coherence length, good tunability, stability, compactness and robustness, with potential impact in optical coherent communications, metrology and sensing.

© 2017 Optical Society of America

OCIS codes: (060.2310) Fiber optics; (140.3540) Lasers, Q-switched; (190.4400) Nonlinear optics, materials.

References and links

1. K. S. Novoselov, A. K. Geim, S. V. Morozov, D. Jiang, M. I. Katsnelson, I. V. Grigorieva, S. V. Dubonos, and A. A. Firsov, "Two-dimensional gas of massless Dirac fermions in graphene," *Nature* **438**(7065), 197–200 (2005).
2. R. R. Nair, P. Blake, A. N. Grigorenko, K. S. Novoselov, T. J. Booth, T. Stauber, N. M. R. Peres, and A. K. Geim, "Fine structure constant defines visual transparency of graphene," *Science* **320**(5881), 1308 (2008).
3. F. Bonaccorso, Z. Sun, T. Hasan, and A. C. Ferrari, "Graphene photonics and optoelectronics," *Nat. Photonics* **4**(9), 611–622 (2010).
4. F. J. García de Abajo, "Graphene nanophotonics," *Science* **339**(6122), 917–918 (2013).
5. K. S. Novoselov, V. I. Fal'ko, L. Colombo, P. R. Gellert, M. G. Schwab, and K. Kim, "A roadmap for graphene," *Nature* **490**(7419), 192–200 (2012).
6. A. N. Grigorenko, M. Polini, and K. S. Novoselov, "Graphene plasmonics," *Nat. Photonics* **6**(11), 749–758 (2012).
7. Z. Q. Li, E. A. Henriksen, Z. Jiang, Z. Hao, M. C. Martin, P. Kim, H. L. Stormer, and D. N. Basov, "Dirac charge dynamics in graphene by infrared spectroscopy," *Nat. Phys.* **4**(7), 532–535 (2008).
8. K. I. Bolotin, K. J. Sikes, Z. Jiang, M. Klima, G. Fudenberg, J. Hone, P. Kim, and H. L. Stormer, "Ultrahigh electron mobility in suspended graphene," *Solid State Commun.* **146**(9–10), 351–355 (2008).
9. E. Hendry, P. J. Hale, J. Moger, A. K. Savchenko, and S. A. Mikhailov, "Coherent nonlinear optical response of graphene," *Phys. Rev. Lett.* **105**(9), 097401 (2010).

10. G. K. Lim, Z. L. Chen, J. Clark, R. G. S. Goh, W. H. Ng, H. W. Tan, R. H. Friend, P. K. H. Ho, and L. L. Chua, "Giant broadband nonlinear optical absorption response in dispersed graphene single sheets," *Nat. Photonics* **5**(9), 554–560 (2011).
11. F. Schedin, A. K. Geim, S. V. Morozov, E. W. Hill, P. Blake, M. I. Katsnelson, and K. S. Novoselov, "Detection of individual gas molecules adsorbed on graphene," *Nat. Mater.* **6**(9), 652–655 (2007).
12. Q. L. Bao, H. Zhang, B. Wang, Z. H. Ni, C. H. Y. X. Lim, Y. Wang, D. Y. Tang, and K. P. Loh, "Broadband graphene polarizer," *Nat. Photonics* **5**(7), 411–414 (2011).
13. F. Wang, Y. Zhang, C. Tian, C. Girit, A. Zettl, M. Crommie, and Y. R. Shen, "Gate-variable optical transitions in graphene," *Science* **320**(5873), 206–209 (2008).
14. M. Liu, X. Yin, E. Ulin-Avila, B. Geng, T. Zentgraf, L. Ju, F. Wang, and X. Zhang, "A graphene-based broadband optical modulator," *Nature* **474**(7349), 64–67 (2011).
15. C. T. Phare, Y. H. D. Lee, J. Cardenas, and M. Lipson, "Graphene electro-optic modulator with 30 GHz bandwidth," *Nat. Photonics* **9**(8), 511–514 (2015).
16. S. Chakraborty, O. P. Marshall, T. G. Folland, Y. J. Kim, A. N. Grigorenko, and K. S. Novoselov, "Gain modulation by graphene plasmons in aperiodic lattice lasers," *Science* **351**(6270), 246–248 (2016).
17. W. Li, B. Chen, C. Meng, W. Fang, Y. Xiao, X. Li, Z. Hu, Y. Xu, L. Tong, H. Wang, W. Liu, J. Bao, and Y. R. Shen, "Ultrafast all-optical graphene modulator," *Nano Lett.* **14**(2), 955–959 (2014).
18. C. Meng, S. L. Yu, H. Q. Wang, Y. Cao, L. M. Tong, W. T. Liu, and Y. R. Shen, "Graphene-doped polymer nanofibers for low-threshold nonlinear optical waveguiding," *Light Sci. Appl.* **4**(11), e348 (2015).
19. J. H. Chen, B. C. Zheng, G. H. Shao, S. J. Ge, F. Xu, and Y. Q. Lu, "An all-optical modulator based on a stereo graphene–microfiber structure," *Light Sci. Appl.* **4**(12), e360 (2015).
20. F. Xia, T. Mueller, Y. M. Lin, A. Valdes-Garcia, and P. Avouris, "Ultrafast graphene photodetector," *Nat. Nanotechnol.* **4**(12), 839–843 (2009).
21. B. C. Yao, Y. J. Rao, Z. N. Wang, Y. Wu, J. H. Zhou, H. Wu, M. Q. Fan, X. L. Cao, W. L. Zhang, Y. F. Chen, Y. R. Li, D. Churkin, S. Turitsyn, and C. W. Wong, "Graphene based widely-tunable and singly-polarized pulse generation with random fiber lasers," *Sci. Rep.* **5**, 18526 (2015).
22. T. Gu, N. Petrone, J. F. McMillan, A. van der Zande, M. Yu, G. Q. Lo, D. L. Kwong, J. Hone, and C. W. Wong, "Regenerative oscillation and four-wave mixing in graphene optoelectronics," *Nat. Photonics* **6**(8), 554–559 (2012).
23. D. Rodrigo, O. Limaj, D. Janner, D. Etezadi, F. J. Garcia de Abajo, V. Pruneri, and H. Altug, "Mid-infrared plasmonic biosensing with graphene," *Science* **349**(6244), 165–168 (2015).
24. B. C. Yao, Y. Wu, C. B. Yu, J. R. He, Y. J. Rao, Y. Gong, F. Fu, Y. F. Chen, and Y. R. Li, "Partially reduced graphene oxide based FRET on fiber-optic interferometer for biochemical detection," *Sci. Rep.* **6**, 23706 (2016).
25. A. Martinez and Z. P. Sun, "Nanotube and graphene saturable absorbers for fibre lasers," *Nat. Photonics* **7**(11), 842–845 (2013).
26. K. Wang, J. Wang, J. Fan, M. Lotya, A. O'Neill, D. Fox, Y. Feng, X. Zhang, B. Jiang, Q. Zhao, H. Zhang, J. N. Coleman, L. Zhang, and W. J. Blau, "Ultrafast saturable absorption of two-dimensional MoS₂ nanosheets," *ACS Nano* **7**(10), 9260–9267 (2013).
27. D. Mao, Y. Wang, C. Ma, L. Han, B. Jiang, X. Gan, S. Hua, W. Zhang, T. Mei, and J. Zhao, "WS₂ mode-locked ultrafast fiber laser," *Sci. Rep.* **5**, 7965 (2015).
28. Q. L. Bao, H. Zhang, Y. Wang, Z. H. Ni, Y. L. Yan, Z. X. Shen, K. P. Loh, and D. Y. Tang, "Atomic-layer graphene as a saturable absorber for ultrafast pulsed lasers," *Adv. Funct. Mater.* **19**(19), 3077–3083 (2009).
29. Z. Sun, T. Hasan, F. Torrisi, D. Popa, G. Privitera, F. Wang, F. Bonaccorso, D. M. Basko, and A. C. Ferrari, "Graphene mode-locked ultrafast laser," *ACS Nano* **4**(2), 803–810 (2010).
30. D. Popa, Z. Sun, T. Hasan, F. Torrisi, F. Wang, and A. C. Ferrari, "Graphene Q-switched, tunable fiber laser," *Appl. Phys. Lett.* **98**(7), 073106 (2011).
31. Y. Tang, X. Yu, X. Li, Z. Yan, and Q. J. Wang, "High-power thulium fiber laser Q switched with single-layer graphene," *Opt. Lett.* **39**(3), 614–617 (2014).
32. A. Choudhary, S. J. Beecher, S. Dhingra, B. D'Urso, T. L. Parsonage, J. A. Grant-Jacob, P. Hua, J. I. Mackenzie, R. W. Eason, and D. P. Shepherd, "456-mW graphene Q-switched Yb:yttria waveguide laser by evanescent-field interaction," *Opt. Lett.* **40**(9), 1912–1915 (2015).
33. S. Liu, X. Zhu, G. Zhu, K. Balakrishnan, J. Zong, K. Wiersma, A. Chavez-Pirson, R. A. Norwood, and N. Peyghambarian, "Graphene Q-switched Ho³⁺-doped ZBLAN fiber laser at 1190 nm," *Opt. Lett.* **40**(2), 147–150 (2015).
34. J. Liu, S. Wu, Q. H. Yang, and P. Wang, "Stable nanosecond pulse generation from a graphene-based passively Q-switched Yb-doped fiber laser," *Opt. Lett.* **36**(20), 4008–4010 (2011).
35. U. Keller, "Recent developments in compact ultrafast lasers," *Nature* **424**(6950), 831–838 (2003).
36. B. W. Tilma, M. Mangold, C. A. Zaugg, S. M. Link, D. Waldburger, A. Klenner, A. S. Mayer, E. Gini, M. Golling, and U. Keller, "Recent advances in ultrafast semiconductor disk lasers," *Light Sci. Appl.* **4**(7), e310 (2015).
37. C. Hönninger, R. Paschotta, F. Morier-Genoud, M. Moser, and U. Keller, "Q-switching stability limits of continuous-wave passive mode locking," *J. Opt. Soc. Am. B* **16**(1), 46–56 (1999).
38. M. Chernysheva, C. Mou, R. Arif, M. AlAraini, M. Rummeli, S. Turitsyn, and A. Rozhin, "High power Q-Switched Thulium doped Fibre Laser using carbon nanotube polymer composite saturable absorber," *Sci. Rep.* **6**, 24220 (2016).

39. Y. Chen, C. J. Zhao, S. Q. Chen, J. Du, P. H. Tang, G. B. Jiang, H. Zhang, S. C. Wen, and D. Y. Tang, "Large energy, wavelength widely tunable, topological insulator Q-switched erbium-doped fiber laser," *IEEE J. Sel. Top. Quantum Electron.* **20**(5), 0900508 (2014).
40. T. Jiang, Y. Xu, Q. J. Tian, L. Liu, Z. Kang, R. Y. Yang, G. S. Qin, and W. P. Qin, "Passively Q-switching induced by gold nanocrystals," *Appl. Phys. Lett.* **101**(15), 151122 (2012).
41. R. I. Woodward, E. J. R. Kelleher, R. C. T. Howe, G. Hu, F. Torrisi, T. Hasan, S. V. Popov, and J. R. Taylor, "Tunable Q-switched fiber laser based on saturable edge-state absorption in few-layer molybdenum disulfide (MoS₂)," *Opt. Express* **22**(25), 31113–31122 (2014).
42. J. Liu, X. Tian, K. Wu, Q. Dai, W. Han, and H. Zhang, "Highly efficient Q-switched laser operation of Yb:Y3Ga5O12 garnet crystal," *Opt. Express* **21**(3), 2624–2631 (2013).

1. Introduction

Two-dimensional materials, especially graphene and its derivatives [1,2], have attracted worldwide interests, due to their exceptional optical and electronic properties [3–5]. Specifically, based on its polarization dependent transmission [6], Fermi level tunability [7], ultrahigh carrier mobility [8], broadband high-nonlinearity [9,10], and surface sensitivity [11], a full range of graphene-based optoelectronic devices have been reported [12–24]. In recent years, advanced saturable absorbers based on two-dimensional materials including graphene, WS₂ and MoS₂ have shown intriguing properties [25–27], and brought considerable breakthroughs for mode-locked lasers [28,29] and Q-switched lasers [30–33]. Moreover, due to their atomically thin layer topology, the saturable absorbers have compatibility with optical waveguides and fibers. In particular, graphene-based passive Q-switched fiber laser has been heavily investigated recently to fulfill its promise as a compact, low-cost, and flexible light source for nanosurgery, environmental sensing, holographic metrology and coherent LIDAR [34,35].

Here we demonstrate single-frequency Q-switching, for the first time, in a compact graphene-coated DFB fiber laser (GDFB-FL). The short cavity and DFB configuration not only increase the laser stability against the ambient disturbance but also ensure single longitudinal mode operation resulting in a low noise pulse shape and a narrow laser linewidth. Thus the all-optical passive Q-switching generates μ s pulses in the monolayer graphene DFB-FL, with up to 10 nJ pulse energies and hundreds of kHz spectral linewidths simultaneously. The pulses are near transform-limited and with kHz repetition rates. By further optimizing the cavity structure and graphene coating, the Q-switched GDFB-FL can generate pulses with sub-100 ns pulse duration and more than MHz repetition rates. The single frequency, narrow linewidth Q-switched centimeter-scale GDFB-FL with good tunability, stability in an all-fiber robust implementation is suitable for applications in coherent fiber communications and sensing, holographic metrology and coherent LIDAR where a long coherence length is preferable.

2. Results

Figures 1(a) and 1(b) shows the GDFB-FL schematically. A 4.5 cm long π phase-shifted DFB is written in a 6 cm long photosensitive Er³⁺ doped fiber, forming a DFB fiber laser. A 1 cm long section in the middle of the DFB is chemically etched by using buffered oxide etch (BOE). The cladding in etched section is etched to ~ 2 μ m, and the core diameter of the Er³⁺ doped fiber is 8 μ m. Monolayer graphene is grown on copper foil through chemical-vapor deposition (CVD), and wrapped around the etched section of the DFB via the wet transferring technique, with a length of ~ 5 mm. Details of the fabrication process are shown in the Appendix. Characterization of the GDFB-FL is demonstrated in Figs. 1(c)-1(e). Figure 1(c) illustrates the GDFB-FL when a 635 nm light is launched in the fiber laser. The graphene coated area is bright, due to impedance mismatch and stronger higher-order fiber mode excitation. Figure 1(d) shows the microscope image at the boundary of the graphene coating on the etched DFB. Figure 1(e) illustrates the Raman spectrum of the pre- and post-transfer CVD graphene coated on the fiber. The narrow G peak, strong 2D peak along with negligible D peak suggest high-quality graphene even after transfer.

With finite-element simulations (COMSOL), we model the fundamental modal E -field distribution of the DFB, etched DFB, and GDFB as shown in Fig. 1(f). With the etched cladding, the evanescent field extends further out of the core, and interacts stronger with the coated graphene. The corresponding computed fundamental modal effective indices of the DFB, etched DFB and GDFB are 1.4569, 1.4551, and 1.4545 respectively.

Figure 1(g) demonstrates the lasing spectra of the DFB, etched-DFB, and GDFB on an optical spectral analyzer (ANDO AQ6317, resolution of 10 pm), pumped by a 980 nm CW diode with 60 mW power. The original DFB fiber laser has a peak location at 1547.4 nm, and 78 μ W (−11.1 dBm) averaged output power. After etching and due to the smaller effective index, the peak location of the etched DFB shifts to 1545.3 nm. The small peaks on the higher frequency edge are due to the very weak higher-order mode excitation and generation. The etched DFB has $\sim 42 \mu$ W (−13.8 dBm) averaged output power. After coating with monolayer graphene, the loss of the etched-DFB is further increased, resulting in an average 0.9 μ W (−30.5 dBm) output power. The peak of the GDFB-FL is further blue-shifted to 1544.5 nm. Optical absorption of the graphene brings serious loss, which would be modulated periodically in the Q -switching. In future, by controlling the etching process better and decreasing the graphene induced scattering, the intrinsic loss could be further optimized.

By using a 30 km fiber delay line, we measured the linewidth of the laser based on the self-heterodyne technique while keeping the pump at 60 mW, as shown in the Appendix. The self-beating results on the electronic spectrum analyzer are subsequently shown in Fig. 1(h). Initially the DFB laser we adopted has a ~ 2.5 kHz full-width half-maximum (FWHM) linewidth. Etching induces additional loss and broadens its linewidth to be ~ 5.5 kHz. At 60 mW, the pump power is just near the threshold for Q -switching the GDFB-FL, with the GDFB-FL output power less than 1 μ W and is unstable for rigorous linewidth measurements.

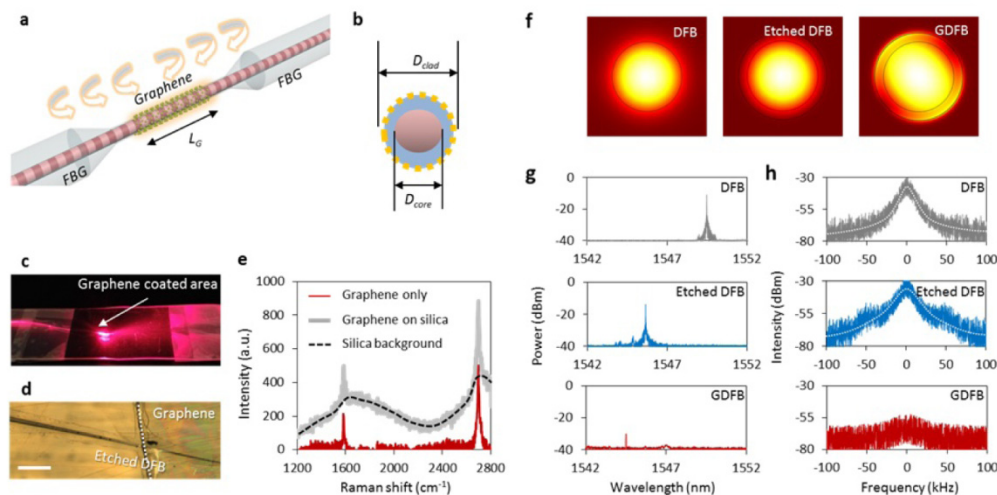


Fig. 1. Structure of the graphene-based DFB fiber laser (GDFB-FL). (a) Schematic diagram of the GDFB-FL. (b) Sectional view. (c) Optical image of the GDFB-FL, with 635 nm launched laser for visualization. (d) Microscope image of the GDFB-FL, with graphene boundary marked by white dashed curve. Scale bar: 100 μ m. (e) Raman spectra of CVD graphene on the GDFB-FL. The grey curve shows the spectrum with a background noise (black dashed), while the red curve shows the filtered spectrum. (f) Simulated $|E|$ -field of fundamental mode of the DFB, the etched DFB, and the GDFB. (g) and (h), Under continuous-wave 980 nm pump at 60 mW, the respective laser spectra and beating linewidths of the DFB (grey), the etched DFB (blue) and the GDFB (red). In (h), the white curves are the Lorentzian fits.

We next drive the GDFB-FL into passive Q -switching as shown in Fig. 2. Figure 2(a) shows the experimental setup. Pump light from a tunable 980 nm laser module (maximum

power 157 mW) is launched in the GDFB-FL via a 980/1550 WDM (bandwidth ~ 100 nm). Backward 1550 nm lasing is collected via the WDM. We measured the GDFB-FL spectral and temporal properties by using a high resolution optical spectrum analyzer (Advantest Q8384), an electronic spectrum analyzer (Agilent N9000A), and an oscilloscope (RIGOL DS1054).

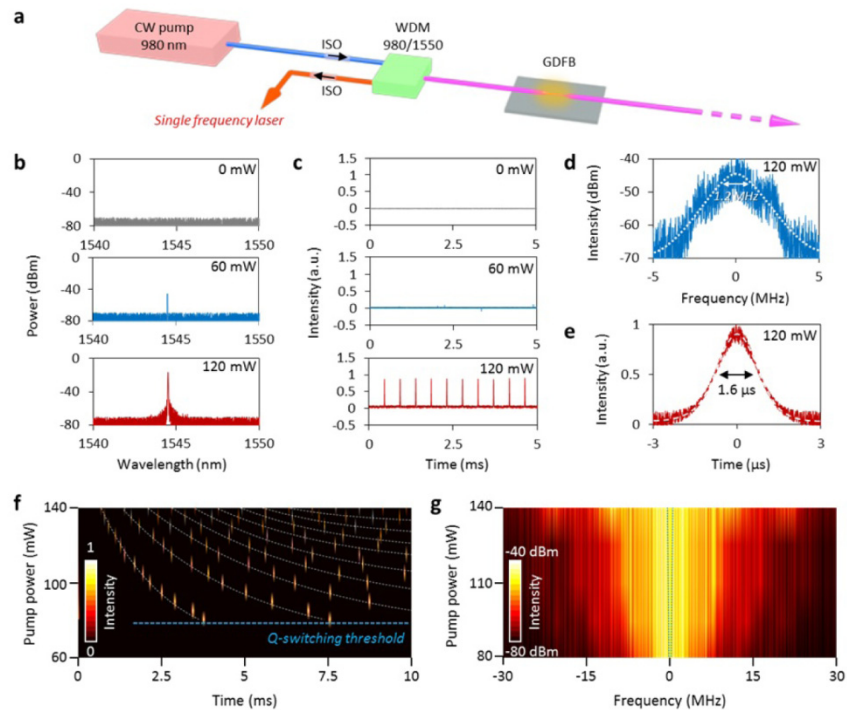


Fig. 2. Passively Q -switched GDFB-FL. (a) Experimental setup. (b) and (c), Spectra and temporal profiles of the GDFB-FL at pump power of 0 mW (grey), 60 mW (blue), and 120 mW (red). (d) Linewidth of the beating, which is a sum of the Q -switched GDFB-FL linewidth (~ 700 kHz) and a reference (~ 500 kHz) at pump power of 120 mW. The dashed white curve shows the Lorentzian fitting. (e) Zoom-in of a pulse of the Q -switched GDFB-FL at pump power of 120 mW. Here the black dashed curve shows the Gaussian fitting. In panels (c) and (e), intensities are normalized. (f) Measured map of the pulses, under pump power in range of 80 mW to 140 mW. Here the pulse energy is normalized and the white dashed curves are fittings. (g) Measured beating spectrum of the GDFB-FL. Here the blue dashed curve shows the 3 dB linewidth.

Figure 2(b) shows the spectral evolution when pumped with increasing power from 0 mW to 120 mW. When the pump power reaches 54.7 mW (threshold), lasing at 1544.5 nm is observed. With the pump power from 54.7 mW to ~ 78.6 mW, the GDFB-FL output is of CW operation with a weak and unstable lasing output, as the saturable absorption of the graphene cladding is not obvious. For example, in the middle panel of Fig. 2(c) (the temporal profile) with 60 mW pump, the GDFB-FL weak CW output starts to illustrate nascent intensity fluctuations, at the onset of Q -switching. Once the pump power is higher than ~ 78.6 mW, Q -switching begins to occur distinctly. As illustrated in the third (red line) panel of Fig. 2(c) with 120 mW pump, the train of pulses is clearly observed and an average lasing power of 20 μ W (-17 dBm) is achieved. Above threshold, the energy in the DFB cavity saturates the graphene, and a stable Q -switched pulse train is formed. The repetition rate of this pulse train is 2.16 kHz, and the signal-noise-ratio (SNR) of the pulse is higher than 20 dB. By increasing the pump power, the output SNR could be further improved.

With the pulse formation in the Q -switched GDFB-FL, instead of using self-heterodyning to measure the linewidth, we heterodyne beat the GDFB-FL with a stable narrow-linewidth tunable CW laser (Santec TSL-710) as the reference. The reference laser linewidth is ~ 500 kHz. Figure 2(d) illustrates the beating linewidth of the Q -switched GDFB-FL under a 120 mW pump. The FWHM linewidth of the 120 mW pumped pulsed GDFB-FL is ~ 700 kHz. Figure 2(e) shows a zoomed-in pulse. The pulse duration is ~ 1.6 μ s, and the pulse energy reaches 10 nJ. In such a compact laser cavity, the temporal profile could be well-fitted with a Gaussian pulse shape. We also note that in the passively Q -switched GDFB-FL, the pulse duration is mainly determined by the energy accumulation rate of the GDFB cavity, which is much slower than the intrinsic carrier dynamics of graphene. In Figs. 2(b)-2(e), the pump power is fixed at 120 mW, to control the thermal noise and spectral instabilities.

Figure 2(f) shows the measured pulses of the GDFB-FL, mapped with the pump power. Every bright point in the figure represents a single pulse. With pump power increasing from 80 mW to 140 mW, the repetition rate is tuned over $5.4 \times$, from ~ 0.7 kHz to ~ 3.8 kHz while the pulse duration is shortened from ~ 7 μ s to ~ 1 μ s. Correspondingly, Fig. 2(g) shows the modification of the heterodyne beat RF spectrum for increasing pump. With increasing pump power, the linewidth of the GDFB-FL increases from ~ 700 kHz to ~ 900 kHz, fairly constant.

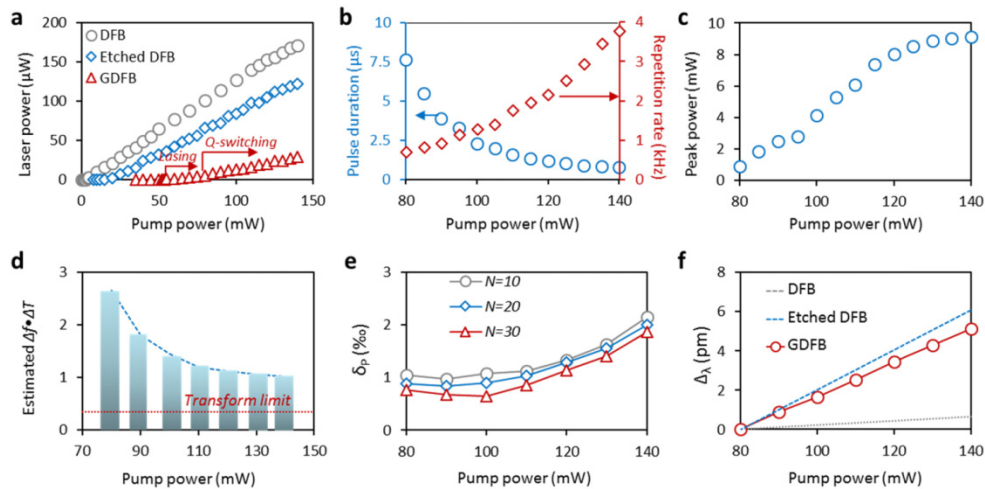


Fig. 3. Properties of the passively Q -switched GDFB-FL. (a) Pump-laser power correlations of the DFB (gray dots), the etched DFB (blue diamonds), and the GDFB (red triangles) lasers. The maximum energy transfer efficiency of the DFB, etched DFB and GDFB lasers are 1.3%, 0.7%, and 0.18%, respectively. (b) Measured correlation of pulse durations (blue dots) and repetition rates (red diamonds) of the GDFB-FL versus pump power. (c) Peak power of the GDFB-FL. (d) Measured $Af \cdot \Delta T$ product of the Q -switched GDFB-FL. The red dashed line marks the theoretical transform limit. (e) and (f) Temporal instability and spectral drift of the GDFB-FL, varying with pump power.

Figure 3 summarizes the properties of the passively Q -switched GDFB-FL. In Fig. 3(a), we compare the pump-output intensity correlations of the DFB, etched DFB, and GDFB-FL. In Q -switched lasers, energy conversion efficiency is determined by both the gain media and the cavity Q -factor. Because of the graphene-induced optical adsorption, the GDFB-FL has a lower lasing efficiency but a higher threshold. That means, stimulated by the same pump, the GDFB-FL has the lowest average power. The efficiency of the DFB, etched DFB, and GDFB laser are determined to be 1.3%, 0.7%, and 0.18% respectively. However, the GDFB-FL begins to be Q -switched once the pump power is greater than 78.6 mW. With increasing pump power, the repetition rate increases and the pulse duration decreases as shown in Fig. 3(b), limited only by the maximum output power of our 980 nm pump. Based on the measured results, we calculate the peak power of the GDFB-FL as illustrated in Fig. 3(c).

When the launched pump power reaches 140 mW, the peak power of the passively Q -switched GDFB-FL approaches 10 mW. With a pulse duration of $\sim 1.6 \mu\text{s}$, the pulse energy is $\sim 10 \text{ nJ}$. Figure 3(d) next shows the $\Delta f \cdot \Delta T$ product of the passively Q -switched GDFB-FL, which reflects the energy balance of a pulsed laser in both frequency and time domains. Here, Δf and ΔT are the spectral FWHM and the pulse FWHM respectively. With the pump increases from 80 mW to 140 mW, the $\Delta f \cdot \Delta T$ decreases from 2.7 to 0.9, close to the Fourier transform limit (0.44 for Gaussian pulses).

We also investigate the instability of the passively Q -switched GDFB-FL, as shown in Fig. 3(e). We define the intensity instability of the pulse train as δ_p in Eq. (1). Here N is the number of the pulses, I_i is the intensity of a single pulse, I_{ave} is the average intensity of the pulse train. With increasing the pump power, δ_p decreases initially, then increases back, with a minimal pulse-to-pulse intensity instability of 0.65% at 100 mW pump power. When the pump power is higher than 100 mW, thermal instability from the pump would increase δ_p . Spectral drift of the passively Q -switched GDFB-FL is further shown in Eq. (2) and Fig. 3(f). The location of the laser peak is determined by the Bragg grating period in the DFB cavity. When the pump power increases, the GDFB expands thermally, leading to the red shift in the output peak wavelength. In Eq. (2), λ_i is a central wavelength at each pump power and λ_o is the initial peak location of the GDFB at 1544.4984 nm under 80 mW pump.

$$\delta_p = \frac{\sum_{i=1}^N (I_i - I_{ave})^2}{N} \quad (1)$$

$$\Delta_\lambda = \lambda_i - \lambda_o \quad (2)$$

As shown in Fig. 3(f), increasing the pump power can also influence the central peak location of the GDFB-FL, as the Bragg gratings are thermally sensitive. $\Delta\lambda$ of the GDFB-FL is measured to be 80 fm per mW pump. Consequently, with a stabilized pump power, the GDFB-FL can be relatively stable in both intensity and central wavelength. In the measurement, the amplitude instability is $< 1\%$ in 2 hours. To further optimize this issue, applying a temperature controller is also a good choice.

3. Discussions

To further understand the measurements of Figs. 2 and 3, we theoretically analyze the factors determining the pulse duration, repetition rate and spectral linewidth of the passive Q -switched GDFB-FL. The effective cavity length of the GDFB-FL L_c is $\sim 4.5 \text{ cm}$, thus the round-trip time of this cavity T_R is $\sim 0.5 \text{ ns}$. Referring Lasing dynamics theory [36], with a fixed pump at 120 mW, Fig. 4(a) simulates the lasing dynamics of the GDFB-FL. With a τ_g of $\sim 220 \text{ fs}$, the generated Q -switched pulses are of 2.17 kHz repetition rate and modeled pulse duration is $1.4 \mu\text{s}$, corresponding remarkably well to our measurements. Moreover, we investigate the possibility to Q -switch the GDFB-FL at higher repetition rates. Figure 4(b) maps how the DFB cavity design influences the repetition rate, via varying the intracavity gain and the round-trip time. By increasing the DFB lasing efficiency (e.g. using highly-doped Er3 + fiber) or decreasing the round-trip time (e.g. shortening the cavity), the passively Q -switched GDFB-FL can achieve a higher repetition rate. Furthermore, Fig. 4(c) illustrates that the pulse duration could be further modulated by tuning the graphene characteristics. By doping or gating [14, 22] graphene, τ_g and α could be modified, resulting in control and tuning of the output pulse duration.

In Figs. 4(d)-4(f), we map and compare the Q -switched GDFB-FL and the previously reported graphene based mode-locked / Q -switched fiber lasers. Here Ref [37–42]. are shown in the Fig. 4(f). As Fig. 4(d) shows, conventional graphene mode-locked fiber lasers often have sub ps pulsewidth temporally and hundreds GHz linewidth spectrally, while conventional graphene Q -switched fiber lasers have 10^2 ns level pulsewidth and hundreds GHz linewidth as well. Limited by their long fiber cavities (usually in meter level), their

lasing operation are far away from transform limit. In the Q -switched GDFB-FL, the compact cavity in a single centimeters long fiber section enables sub MHz linewidth for Q -switched pulses stably, orders narrower than the conventional graphene pulsed lasers. As Fig. 4(e) shows, for a mode-locked fiber laser, as the pulsewidth is considerably narrow, its pulse energy is limited. In comparison, the Q -switched fiber lasers including the Q -switched GDFB-FL can output orders higher energy pulses with widely tunability, which is significant for many practical applications. The comparison shown in Fig. 4(f) also illustrates that related to conventional Q -switched lasers by using graphene, our compact GDFB-FL has a very low absorbed pump threshold (< 4 mW). In sum, the Q -switched GDFB-FL, an unpredicted miniature optical laser device, has unique physical response both spectrally and temporally, showing new potentials in graphene fast optics.

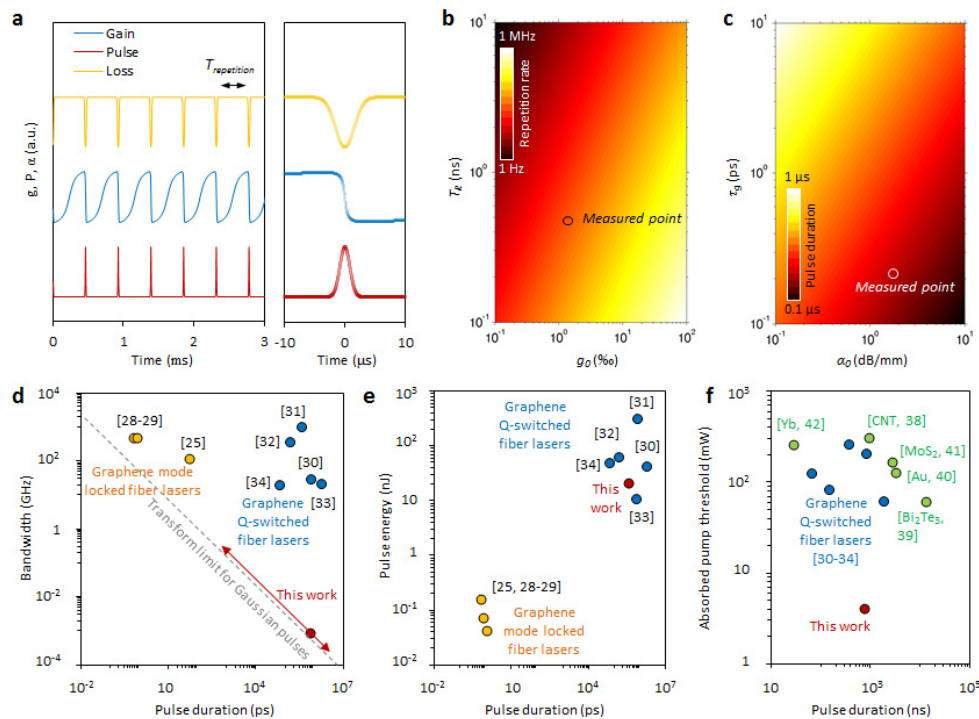


Fig. 4. Discussions. (a) Left column: Calculated round-trip gain $g(t)$ (blue), transient laser power $P(t)$ (red), and round-trip graphene absorption $\alpha(t)$ (grey) in the passive Q -switching. All curves are normalized. Right column: Zoomed in temporal profiles, around the center of a single pulse. (b) Simulated map of the repetition rate, depending on the small-signal round-trip gain g_0 and round-trip cavity time T_R . Here the experimentally measured parameter in the earlier Fig. 2(c) with repetition rate of 2.16 kHz is marked. (c) Simulated map of the pulse duration, relying on α_0 and τ_g . Here the experimentally parameter with pulse duration of 1.6 μ s in the earlier Fig. 2(e) is marked. (d) to (f), 2D maps compares the pulse durations vs bandwidths, the pulse durations vs pulse energies, and the pulse durations vs absorbed pump threshold. Here the red arrow shows the tunable potential analyzed in (b) & (c). Here red dot shows this work, yellow dots show the examples of graphene mode-locked fiber lasers and Q -switched fiber lasers respectively. In f, green dots show the Q -switched lasers applying other saturable absorbers.

4. Summary

In this work we proposed and demonstrated graphene passive Q -switching in a narrow linewidth distributed feedback Bragg-grating fiber laser, approaching the transform limit. In the Q -switched GDFB-FL, determined by the graphene-based saturable absorption in the

stable laser cavity, high quality pulses are generated and controlled by tuning the pump power. The Q -switched GDFB-FL provides ~ 10 nJ pulse energies, with μ s pulse durations and sub-MHz spectral linewidths. Experimentally the repetition rate is tuned over $5.4 \times$ via the pump power control, while the pulse-to-pulse intensity fluctuation is observed to be 0.65% at 100 mW pump. By optimizing the intracavity round-trip time, gain efficiency, graphene cladding recovery time and absorption rate, the Q -switching can work with greater than MHz repetition rates while affording ns pulse durations. The switchable all-in-line GDFB-FL is highly compact and robust, for planar waveguide DFB laser integration towards long-distance coherent fiber communication and distributed fiber-optic sensing, imaging, and spectroscopy.

Appendix

The fabrication process of the GDFB-FL is shown in Fig. 5. First, a 4.5 cm long DFB is written in a 6 cm long photosensitive erbium-doped fiber (EDF, Nufern 980Hp), to form the DFB fiber laser. The grating is written by scanning a 244 nm frequency-doubled harmonic argon ion laser across the phase mask and fiber. The phase mask is fixed on a piezoelectric transducer stage (PI, P-752.11c) with nanometer resolution. The displacement of the phase mask for an accurate $\pi/2$ phase shift is a quarter of the phase mask period. Second, the DFB fiber laser is etched by the buffered oxide etch (BOE), which contains hydrofluoric acid (HF, 1:6) for 1.5 hours. The etching rate is checked several times during the etching process, ensuring the etching accuracy. In the etching process, the DFB fiber laser was fixed on a plastic substrate. Third, monolayer graphene grown on Cu foil by CVD method is spin-coated by poly (methyl methacrylate) [PMMA]. Subsequently the Cu foil is removed with 1M FeCl₃ solution. After DI water rinsing, the PMMA-graphene hybrid film is coated on the etched DFB fiber laser. The excess graphene is cut off. Finally the PMMA was removed by acetone to form the GDFB-FL. The GDFB-FL is cleaned by water and dried at room temperature.

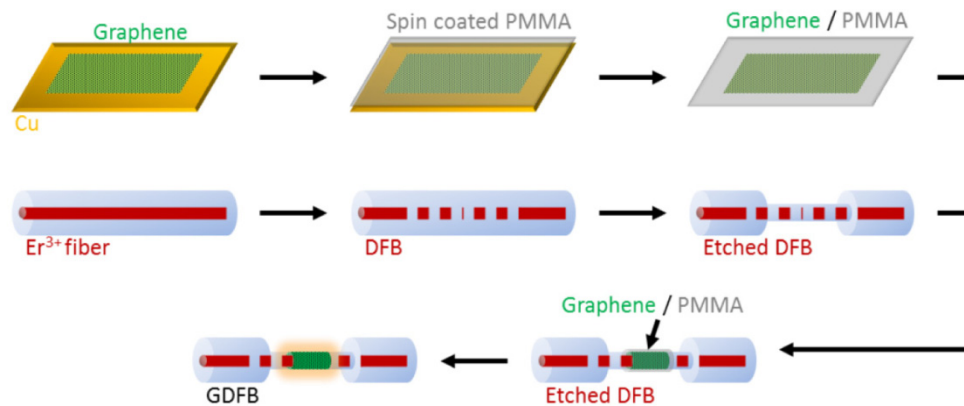


Fig. 5. Fabrication process of the GDFB-FL. Graphene is grown by using CVD method and transferred to the DFB, which is etched first via BOE approach.

The spectral resolution of typical OSAs is ~ 10 pm (single GHz level), which cannot be applied to measure the narrow linewidth lasers, with MHz level linewidth or less. In this case, heterodyne method is considered. The schemes to measure the linewidth of the DFB-FL and the GDFB-FL are illustrated in Fig. 6. To measure the DFB-FL with CW output, the self-heterodyne method is adopted. To measure the passively Q -switched GDFB-FL with pulsed output (especially when the repetition rate of the passively Q -switched GDFB-FL is only several kHz), using a stable CW laser to beat with the GDFB-FL is necessary. Here we use a stable narrow linewidth CW laser diode as the reference (Santec TSL-710). In the heterodyne beatnote measurements, the optical polarizations are carefully controlled to ensure good

interference. The photodetector used in our experiment has 1.25 GHz bandwidth (PD, Thorlabs, DET01CFC).

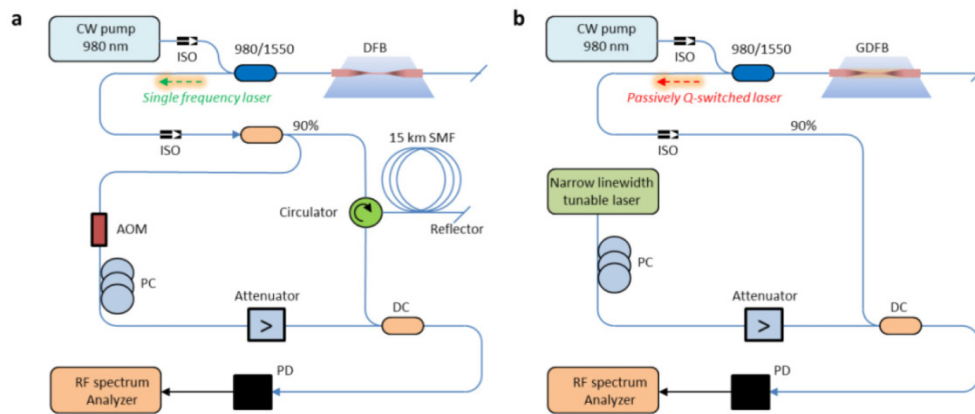


Fig. 6. Measuring the linewidth of the CW DFB-FL and the passively Q -switched GDFB-FL. (a) Self-heterodyne method to measure the linewidth of the DFB-FL and etched DFBFL, which are of CW operation. (b) Heterodyne method to measure the linewidth of the GDFBFL, which is Q -switched. Here the RF-spectrum analyzer has a range of 9 kHz to 3 GHz; and a resolution of 10 Hz is applied. Tunable range of the narrow linewidth tunable laser is 1480 nm to 1620 nm, with minimum linewidth 500 kHz.

Funding

This work is supported by the 111 Project (B14039), the China Scholarship Council Grant 201506070043, the National Natural Science Foundation of China under Grant 61475032, and the National Science Foundation CBET-1438147.

Acknowledgements

We acknowledge helpful discussions with Bowen Li, Zhenda Xie, Yongnan Li, and Yi-Ping Lai. We thank the Nanolab and the California Nanosystem Institute (CNSI), University of California, Los Angeles, for the nanofabrication and characterizations.